Journal of Solid State Chemistry **157,** 102–109 (2001)
doi:10.1006/jssc.2000.9044, available online at http://www.idealibrary.com on IDEAL®

# Vibrational Spectroscopic Study of the System $\alpha$-$Co_2SiO_4$–$\alpha$-$Ni_2SiO_4$

Chung-Cherng Lin

*Institute of Earth Sciences, Academia Sinica, Nankang, Taipei, Taiwan, Republic of China*

Received August 18, 2000; in revised form November 1, 2000; accepted December 1, 2000

**$\alpha$-$Co_2SiO_4$ (Co-olivine) and $\alpha$-$Ni_2SiO_4$ (Ni-olivine) can form a continuous series of substitutional solid solutions, in which the *b*-axis shows the largest expansion after substitution of $Co^{2+}$ for $Ni^{2+}$. The linear composition dependences for lattice parameters and vibrational frequencies suggest that the mixing of $\alpha$-$Co_2SiO_4$ and $\alpha$-$Ni_2SiO_4$ are nearly ideal, and both $Co^{2+}$ and $Ni^{2+}$ in the $(Co, Ni)_2SiO_4$ solid solutions distribute randomly over the M1 and M2 sites. Addition of $Co^{2+}$ into $\alpha$-$Ni_2SiO_4$ has significantly weakened the Raman intensity of the system. Together with other transition-metal silicate olivines, the frequencies of the lattice Raman modes appear to have a systematic variation with radius and crystal field stabilization energy of cation in the olivine structure, while the same trend has not been observed in the internal modes of $SiO_4$.** © 2001 Academic Press

***Key Words:*** **silicate olivines; Raman spectroscopy; infrared spectroscopy; crystal field stabilization energy.**

## 1. INTRODUCTION

Silicate olivines (a subgroup of orthosilicate $M_2SiO_4$, $M$ = divalent cation) occur predominantly in igneous rock and have been used as an important composition in some refractory materials, additives in cement concrete, flux and slag conditioner in the steel industry, acid-resistant containers, gritblasting materials, ceramic pigments, and so on.

The structure of silicate olivines can be described as a somewhat distorted hexagonal closest-packed array of oxygen atoms in which one-eighth of the tetrahedral and one-half of the octahedral sites are respectively occupied by cations Si and $M$ (e.g., Mg, Fe). The $MO_6$ octahedral sites can be divided into two kinds, M1 and M2; the former is smaller and more distorted with a site symmetry $\bar{1}$, and the latter is larger with a symmetry $m$ (1). The unequivalent octahedral sites have caused enriching of cations (i.e., cation ordering or site preference) in one of the sites in the olivine-type solid solutions. The extent of cation ordering has been correlated with cation size, site distortion, electronegativity, and crystal field stabilization energy (CFSE) of cation (2–7). Many studies have revealed that $Fe^{2+}$ ions are often slightly enriched in the smaller M1 sites of forsterite (6). It is also found that the cation ordering can be significantly promoted by CFSE (2, 6, 8, 9).

The difference between high spin radii of $Co^{2+}$ and $Ni^{2+}$ with a coordination number of six is the same as that in the $Mg^{2+}$–$Fe^{2+}$ pair (10), and the CFSE of cations in M1 and M2 sites of both Co- and Ni-olivines are nonzero (6). Therefore, it is of interest to study site preference, if any, in the system $\alpha$-$Co_2SiO_4$–$\alpha$-$Ni_2SiO_4$ by means of vibrational spectroscopy and X-ray diffraction. Besides, many studies have indicated that the Raman frequencies of olivine always be changed by addition of solute atoms (7, 11, 12). This suggests that a comparison between Raman frequencies of various olivines may shed light on the possible effects of cation size and CFSE on the vibrations of lattice.

## 2. EXPERIMENTAL

### 2.1. Preparation and Identification of Samples

The mixtures of $SiO_2$, $Co_3O_4$, and NiO in the chosen stoichiometric ratio were used for synthesis of Co- and Ni-olivines and their solid solutions. Reagent grade oxide powders were used in the synthesis to minimize the interference from impurities. The oxides were mixed throughout and pressed into a disc before firing in air. Then the discs were heated at a rate of 10°C/min to the selected temperatures and then were kept isothermally for 20 to 120 h in a box furnace. Finally, the samples were cooled in the furnace by switching off the power. It has been pointed out that Ni-olivine will be decomposed into NiO and $SiO_2$ at temperatures higher than 1500°C (13), but the backward solid-state reaction ($NiO + SiO_2 \rightarrow Ni_2SiO_4$) is slow at lower temperatures. Therefore, the firing period for the synthesis of Ni-olivine below 1500°C needs 100 h at least. The calcination conditions for the synthesis of samples (based on mol% of $Co_2SiO_4$) are 1450°C × 120 h for 0 and 10 mol%, 1440°C × 96 h for 20 and 30 mol%, 1400°C × 72 h for 40 and 50 mol%, 1390°C × 48 h for 60 and 70 mol%, 1380°C × 40 h for 80 and 90 mol%, and 1380°C × 20 h for 100 mol%.

The as-formed samples were polished and then X-rayed (Siemens D5000, CuK$\alpha$) to identify their phases and the



0022-4596/01 $35.00

lattice parameters. Step scan with 0.05°/step and 4 s/step was chosen for X-ray diffraction. The relative ratios of Co to Ni in the as-formed samples were analyzed by electron microprobe analysis (Jeol JXA-8900R at 20 kV and 20 s of collection time under wavelength dispersive spectrum mode).

### 2.2. Raman and Infrared Experiments

The ambient infrared and Raman spectra were collected without using polarization analyzer. The Raman spectroscopic study was carried out on a Renishaw-2000 Raman microprobe, and the backscattering (180°) spectra were collected with the 514.5-nm line from a Coherent Innova 2-W argon ion laser. The spectra were recorded with a Leitz UM 20 microscope objective and three accumulations at 60 s integration time with ~120 mW power on the sample. The focused laser spot on the sample was estimated to be 6–8 μm in diameter. Wavenumbers are accurate to $\pm 1\ cm^{-1}$ as determined from plasma emission lines. Each Raman frequency reported in this work is the average of at least eight measurements.

The infrared spectra were obtained by using a Fourier-transform infrared spectrometer (Bruker, EQUINOX 55). Samples (0.5 wt%) were mixed with KBr, ground by an agate mortar and pestle, and then pressed into a disc for infrared measurement. The scan range is 400–1500 $cm^{-1}$, and 32 scans with 2 $cm^{-1}$ resolution were chosen. The frequency of each Raman and infrared band was obtained by Lorentzian curve fitting using the Jandel Scientific Peakfit computer software.

## 3. RESULTS AND DISCUSSION

### 3.1. Characterization of the As-Formed Samples

All the synthetic samples are polycrystalline and transparent. The as-formed $Co_2SiO_4$ crystals are ca. 100–200 μm in size and purple in color, but less than 30 μm in size and yellow-green in color for $Ni_2SiO_4$ crystals. The two end members and their intermediate solid solutions were confirmed by X-ray diffraction to be olivine in crystal structure. On the basis of space group *Pbnm* (62), the lattice parameters are $a = 4.790(1)$, $b = 10.31(1)$, and $c = 6.007(1)$ Å for $Co_2SiO_4$ and $a = 4.734(1)$, $b = 10.133(2)$, and $c = 5.922(2)$ Å for $Ni_2SiO_4$, where values inside the parentheses are standard deviation. These data are close to those reported in previous works (14, 15), though the *a*- and *c*-axes are slightly larger than those reported in literature. For the solid solutions of α-$Co_2SiO_4$ and α-$Ni_2SiO_4$, the crystal size and color are also between the two end members. It is also found that the amount of unreacted NiO, $Co_3O_4$, and $SiO_2$ (cristobalite in phase) increases with decreasing the proportion of $Co_2SiO_4$. This indicates that the presence of $Co^{2+}$ can speed up the formation and crystal growth of the $Co^{2+}$–$Ni^{2+}$ olivines.

Figure 1 shows the composition relationships of lattice parameters, unit cell volume ($V_{cell}$), and the expansion of lattice parameters of the system α-$Co_2SiO_4$–α-$Ni_2SiO_4$. The expansion of lattice parameter is defined to be $100[(m - m_0)/m_0]$, where $m$ and $m_0$ are the parameters of solid solutions and Ni-olivine, respectively. In accordance with Vegard's law (16), these relationships appear to be linear and can be described as follows:

$$a = 4.73 + 0.000568x \text{ (Å)}$$

$$b = 10.14 + 0.00179x \text{ (Å)}$$

$$c = 5.92 + 0.000820x \text{ (Å)}$$

$$V_{cell} = 284.1 + 0.1255x \text{ (Å}^3\text{)},$$

where $x$ = mol% of $Co_2SiO_4$. The difference in cation size between $Co^{2+}$ and $Ni^{2+}$ is only 8%. The crystal structure and charge of cations are the same throughout the whole composition range. Therefore, α-$Co_2SiO_4$ and α-$Ni_2SiO_4$ form a continuous series of substitutional solid solutions at temperatures above 1350°C.

From Fig. 1c, it is obvious that the *b*- and *a*-axes display respectively the largest and the smallest expansion in Ni-olivine after substitution of $Co^{2+}$ for $Ni^{2+}$. That is, substitution of cation shows the weakest effect on the crystal structure along the orientation perpendicular to the $MgO_6$ layer. The *a*-axis also shows the smallest, while the *b*-axis the largest contraction for several olivines under compression (17). These results suggest that the stress caused by substitution of cation and compression is chiefly released via distortion along the *b*-axis, and the linkages parallel to the *b*-axis may be the weakest bondings in average. Therefore, (010) crystallographic face may be the prevailing cleavage plane in Co- and Ni-olivines. The cleavage planes observed in forsterite (Mg-olivine, α-$Mg_2SiO_4$) (1) are consistent with this argument.

### 3.2. Vibrational Spectra

The frequencies and assignments of all infrared and Raman bands observed in this work are listed in Table 1. The corresponding modes of forsterite are also listed. Figures 2 and 3 respectively show the typical ambient infrared and Raman spectra of Co- and Ni-olivines. However, unlike Raman spectrum, most infrared absorptions of the samples showed significant overlap, and thus far larger uncertainties were undergone. Note that only the internal modes of $SiO_4$ were observed in infrared spectra of the present samples in the range of 400–1500 $cm^{-1}$. The absorptions of unreacted $SiO_2$ and NiO observed in the present α-$Ni_2SiO_4$ sample (spectrum **c** in Fig. 2) basically disappear when mole fraction of $Co_2SiO_4$ exceeds 0.1 (spectrum **b** in Fig. 2), indicating

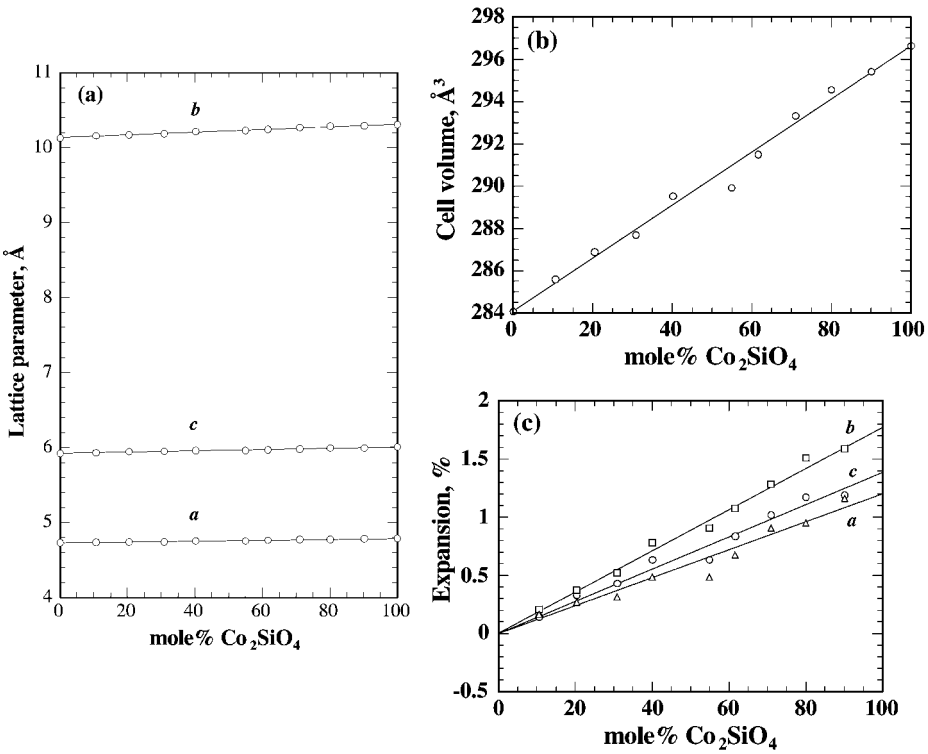


**FIG. 1.** The relationships between composition and (a) lattice parameters $a$, $b$, and $c$, (b) unit cell volume, and (c) the expansion of lattice parameters of $(Co, Ni)_2SiO_4$ solid solutions. The expansion is defined to be $100[(m - m_0)/m_0]$, where $m$ and $m_0$ are the parameters of solid solutions and Ni-olivine, respectively.

that increasing the amount of $Co^{2+}$ is helpful to the formation of $Co^{2+}$–$Ni^{2+}$ olivines. Except difference in frequency, the infrared spectra for all $Co_2SiO_4$–$Ni_2SiO_4$ solid solutions showed the same shape as spectrum **b** in Fig. 2. Similarly, the frequency, intensity, and shape of the Raman spectra for the intermediate solid solutions are between the two end members.

The irreducible representation of olivine is $11A_g + 11B_{1g} + 7B_{2g} + 7B_{3g} + 10A_u + 10B_{1u} + 14B_{2u} + 14B_{3u}$ (18) Thus, a total of 84 vibrational modes is predicted. Among them, 36 modes are Raman active ($A_g$, $B_{1g}$, $B_{2g}$, and $B_{3g}$), 38 are infrared active ($B_{1u}$, $B_{2u}$, and $B_{3u}$), and the $A_u$ modes are both Raman and infrared inactive. The number of Raman and infrared bands that have been observed in Co- and Ni-olivines is far less than predicted. The orientation effect and overlap of absorption bands can be part of the reasons for the scarcity of signals. However, many crystals have been measured, and all samples in this work are polycrystalline. This suggests that weakness of many signals is the crucial factor for lack of bands in a vibrational spectrum of olivines.

The assignments in Table 1 for the modes of Co- and Ni olivines were given by analogy to those for forsterite (19, 20). It is also noteworthy that the assignments of both infrared and Raman modes for olivine in the literature have not reached to be consistent till now. For example, the Raman band of forsterite at 375 $cm^{-1}$ (corresponding to 328 and 344 $cm^{-1}$ in Co- and Ni-olivines, respectively, see Table 1) was also assigned to be mix(Mg, T) — a lattice mode (21), while the strongest Raman bands at 825 and 856 $cm^{-1}$ in forsterite are also assigned to be the mixture of $v_1$ and $v_3$ (22) or $v_3$ for the 825-$cm^{-1}$ band and $v_1$ or $v_2$ for the 856-$cm^{-1}$ band (21, 23).

From Table 1, it is found that except two infrared modes (i.e., 899 and 916 $cm^{-1}$ in Ni-olivine), all the vibrational frequencies of Ni-olivine are higher than those of the corresponding modes of Co-olivine. This case can be attributed to the difference in bond length between the two olivines (i.e., for compounds having the same crystal structure, the smaller in unit-cell volume, the higher in vibrational frequency of the corresponding mode). The two exceptions in infrared modes may partially be attributed to the significant overlap of the absorption bands, which has caused larger uncertainty in data fitting.

On the other hand, the Raman intensity in Ni-olivine is one order of magnitude stronger than that of Co-olivine (Fig. 3), though the crystal size of the latter (ca. 100–200 μm) is far larger than that of the former (< 30 μm). Increasing the amount of $Co_2SiO_4$ has caused weakening in Raman intensity of the system α-$Ni_2SiO_4$–α-$Co_2SiO_4$. On the basis of

**TABLE 1**
**Ambient Infrared and Raman Frequencies for Three Olivines and the Regression Constants Derived from $v = v_0 + ax = bx^2$ (in $cm^{-1}$, $x$ = mol% of $Co_2SiO_4$) for $(Co, Ni)_2SiO_4$ Solid Solutions at Room Temperature and 1 atm**

| | Ambient frequency[a] | | | | | | |
|---|---|---|---|---|---|---|---|
| Assignment[b] | Forsterite | Co-olivine | Ni-olivine | $v_0$ | $a \times 100$ | $b \times 10^4$ | $R^2$ |
| Infrared | | | | | | | |
| $v_4$ | 505 | 482 s | 492 s | 491.5 | 9.40 | | 0.966 |
| $v_4$ | 545 | 514 m sh | 524 m sh | 523.8 | −10.74 | | 0.922 |
| $v_4$ | 614 ± 3 | 573 m sp | 583 m sp | 582.9 | −10.26 | | 0.901 |
| $v_1$ | 841 ± 4 | 822 w sp | 826 w sp | 823.6 | −2.85 | | 0.282 |
| $v_3$ | 892 ± 7 | 867 s | 872 s | 871.3 | −4.62 | | 0.458 |
| $v_3$ | 950 | 900 m sh | 899 m sh | 900.4 | −1.27 | | 0.087 |
| $v_3$ | 961 ± 2 | 920 w sh | 916 w sh | 917.5 | 2.02 | | 0.356 |
| $v_3$ | 995 ± 5 | 950 m | 966 m | 964.7 | −14.09 | | 0.980 |
| X | 1030 ± 70 | 977 m | 984 m | 984.9 | −7.51 | | 0.812 |
| Raman | | | | | | | |
| T | 183 | 135 ± 4 w | | | | | |
| T | 192 | 165 ± 2 w | 181 ± 1 w | 180.8 | −15.36 | | 0.976 |
| T | 226 ± 2 | | 191 ± 2 w | | | | |
| T | 243 ± 1 | 196 w | 221 ± 3 w | 218.5 | −23.78 | | 0.982 |
| T | 305 ± 2 | 248 ± 2 w | 252 ± 2 w | | | | |
| R | 324 ± 2 | | 272 ± 2 w | | | | |
| T | 330 ± 1 | [283] | 298 ± 2 m | 294.9 | −12.06 | | 0.875 |
| R | 366 ± 3 | 295 vw | [332] | 331.8 | −35.04 | | 0.977 |
| R | 375 ± 1 | 328 w | 344 ± 2 w | 348.8 | −21.70 | | 0.830 |
| T | 383 | 336 vw | | | | | |
| $v_2$ | 435 ± 3 | 387 mw | 414 ± 1 m | 417.5 | −29.97 | | 0.976 |
| $v_4$ | 546 ± 2 | 516 ± 1 mw | 521 ± 2 mw | 519.3 | −3.52 | | 0.776 |
| $v_4$ | 593 ± 3 | 552 ± 3 mw | 560 ± 1 ms | 558.9 | −5.92 | | 0.931 |
| $v_4$ | 632 | 573 vw sh | 593 ± 3 m sh | 595.0 | −21.26 | | 0.958 |
| $v_1$ | 825 ± 1 | 811 ± 1 s | 819 ± 1 vs | 818.3 | −7.21 | | 0.956 |
| $v_3$ | 856 ± 1 | 837 ± 1 vs | 839 ± 1 vs | 838.4 | −1.53 | | 0.696 |
| $v_3$ | 882 ± 3 | [855] | 868 ± 2 m sh | 866.7 | −11.24 | | 0.897 |
| $v_3$ | 921 ± 1 | 885 ± 3 mw | 889 ± 3 m | 888.0 | −1.99 | | 0.581 |
| $v_3$ | 966 ± 2 | 928 ± 4 m | 952 ± 2 m | 951.8 | −18.96 | −5.22 | 0.994 |

*Note.* $R^2$ is the coefficient of correlation.

[a]Data of synthetic forsterite are the average of those reported in literature, and data of both Co- and Ni-olivines are from this work. Values in the brackets are obtained from extrapolation. vs, very strong; s, strong; ms, medium to strong; m, medium; mw, weak to medium; w, weak; vw, very weak; sh, should; sp, sharp.

[b]The original assignments of infrared and Raman modes for forsterite can be found in (20) and (19), respectively. For forsterite, only the modes corresponding to those observed in the Co- and Ni-olivines are listed. $v_1$, symmetric $SiO_4$ stretching; $v_2$, symmetric $SiO_4$ deformation; $v_3$, asymmetric $SiO_4$ stretching; $v_4$, asymmetric $SiO_4$ deformation; T, translation; R, rotation, X, overtone/combination.

many measurements, it suggests that this phenomenon is independent of orientation of crystal and laser power. Therefore, the significant weakening in intensity of Raman spectrum can only be correlated to both electronegativity (or electron affinity) and cation mass. The electronegativity of cobalt is smaller than that of nickel, but the inverse for average atomic weight (58.9332 for Co and 58.6934 for Ni). For the $M$–O–Si bondings in Ni-olivine, substitution of Ni by Co may result in smaller reduced mass and dipole moment, though the average length of the $M$–O bond increase after substitution. The two factors cause a smaller polarizability in the vibrations of Co-olivine and thus weaker Raman signals. However, to quantitatively estimate the concentration effect of $Co^{2+}$ on Raman intensity of Ni-olivine, a Raman spectroscopic study should be carried out by collecting spectra from the same crystal orientation in the future.

Figure 4 shows the composition–frequency relationships (i.e., the $X$–$v$ plots) of both infrared and Raman frequencies. It is found that except one Raman mode (952 and 928 $cm^{-1}$ for Ni- and Co-olivines, respectively, also see Table 1), the frequencies of all vibrational modes observed in this work appear to be linear with variation of composition. The regression constants for the $X$–$v$ plots in Fig. 4 are listed in Table 1. The average slope for the $X$–$v$ plots of the lattice modes is larger than that of the $SiO_4$ internal modes,

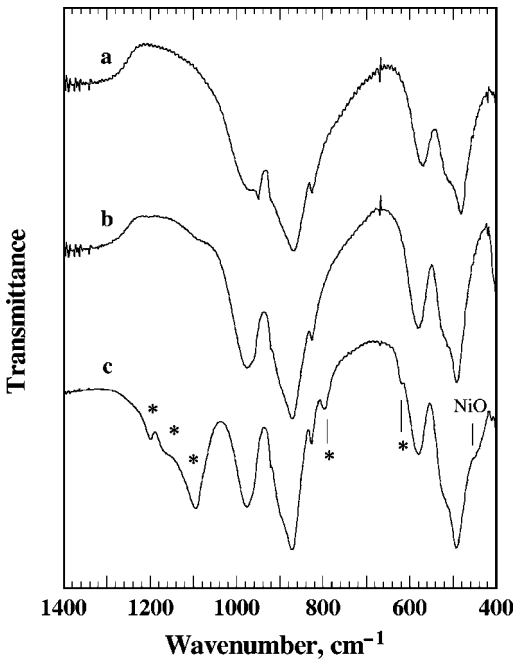


**FIG. 2.** Ambient infrared spectra of (a) Co-olivine, (b) $Co_{1.79}Ni_{0.21}SiO_4$ solid solution, and (c) Ni-olivine. In (c), the absorptions marked by asterisks are the signals of cristobalite (unreacted $SiO_2$), and the shoulder at $\sim 450\ cm^{-1}$ is caused by unreacted NiO.

indicating that the substitution of cation has stronger effect on the lattice vibrations. The nearly linear composition relationship of vibrational frequency has also been observed in most infrared bands of the system $\alpha$-$Mg_2SiO_4$–$\alpha$-$Fe_2SiO_4$ (24).

It should be noted that a small coefficient of correlation ($R^2$) for a set of fitting data can be caused by rather small change in values of data (e.g., a nearly composition-independent relationship of frequency) and/or large scattering in data (i.e., low precision). The former can be observed in a set of highly precise data, whereas the scattering in frequency may result in an apparently weak composition dependence and therefore misjudgment in their relationship. However, most infrared absorptions observed in the present olivine system showed significant overlap (see Fig. 3). Therefore, the conclusion extracted from Raman spectra and the sharp infrared absorptions, which have better $R^2$, should be far more reliable than that based on the highly overlapped infrared bands.

It has been pointed out that a nonlinear $X$–$v$ plot should be obtained if cation ordering occurs in the olivine solid solutions (7, 11, 14). Based on the consideration of larger cation size and smaller CFSE in $Co^{2+}$ (6), one may expect that $Co^{2+}$ has a tendency to be stronger than that of $Ni^{2+}$ for entering the M2 sites. The electrostatic calculations and charge density studies on olivines have suggested that the M2 sites are more ionic than the M1 sites (6), and therefore the more covalent transition metal ions (e.g., $Co^{2+}$ and $Ni^{2+}$) should prefer to reside in the M1 sites of the forsterite-based solid solutions (5, 6, 25, 26). The electron affinity of nickel is stronger than that of cobalt, suggesting that $Co^{2+}$ may enrich in the more ionic M2 site of the $(Co, Ni)_2SiO_4$ solid solutions. If this case is true, the $X$–$v$ plots of the lattice modes in the $(Co, Ni)_2SiO_4$ solid solutions should be concave upward because the Raman frequencies of Co-olivine are lower than that of Ni-olivine. However, the linear frequency–composition relationships should indicate that both $Co^{2+}$ and $Ni^{2+}$ distribute randomly (disordered) over the M1 and M2 sites; that is, cation ordering has never occurred or is negligible in the system $\alpha$-$Co_2SiO_4$–$\alpha$-$Ni_2SiO_4$. In the previous section, it has showed that both lattice parameters and cell volume display linear composition dependences. Therefore, the mixing of cations in $(Co, Ni)_2SiO_4$ olivine solid solutions are nearly ideal.

The reason for disordering of cations in $(Co, Ni)_2SiO_4$ solid solutions is unclear, but may involve a considerable increase in distortion of the M2 octahedra after substitution of $Co^{2+}$ for $Ni^{2+}$. A significant lattice distortion caused by enriching $Co^{2+}$ at the M2 sites should not be favored for sustaining the olivine structure. Besides, it has been revealed that distortions of the M1 and M2 octahedra increase with increasing temperature—the thermal-induced distortion of the M1 sites is more than that of the M2 sites (27–29). This case implies that synthesis of the $(Co, Ni)_2SiO_4$ solid solutions at higher temperature (e.g., the high-$Ni^{2+}$ olivines in this work) is favored for $Co^{2+}$ to enter the M2 site. Therefore, thermal history of the samples should not be the cause for disordering of cations in the system $\alpha$-$Co_2SiO_4$–$\alpha$-$Ni_2SiO_4$.

### *3.3. A Comparison between Various Silicate Olivines*

In the silicate olivines, the $SiO_4$ tetrahedron shares its edges with two M1 octahedra and one M2 octahedron (4, 30), and the M1-related lattice vibrations are Raman inactive (7). The $X$–$v$ slope of the lattice modes is generally steeper than that of the $SiO_4$-internal modes (see Fig. 4 and Table 1). These indicate that the lattice modes (involving only the M2 octahedra) is more suitable than the $SiO_4$-internal modes for observing the effect of cation substitution on Raman frequencies of olivine.

The quality of ambient Raman spectra of forsterite, Ni-olivine, and calcio-olivine ($\gamma$-$Ca_2SiO_4$) is much better than that of fayalite ($\alpha$-$Fe_2SiO_4$), tephroite ($\alpha$-$Mn_2SiO_4$), and Co-olivine, the last three olivines show only several Raman bands (see also Table 1). Therefore, only a few lattice modes can be used to observe the effect of cations. Figure 5 shows five Raman frequencies for six olivines. The vibrational frequencies in Fig. 5 are the average of data obtained from literature and this work. Numbers 1, 2, 3, 4, and 5 represent

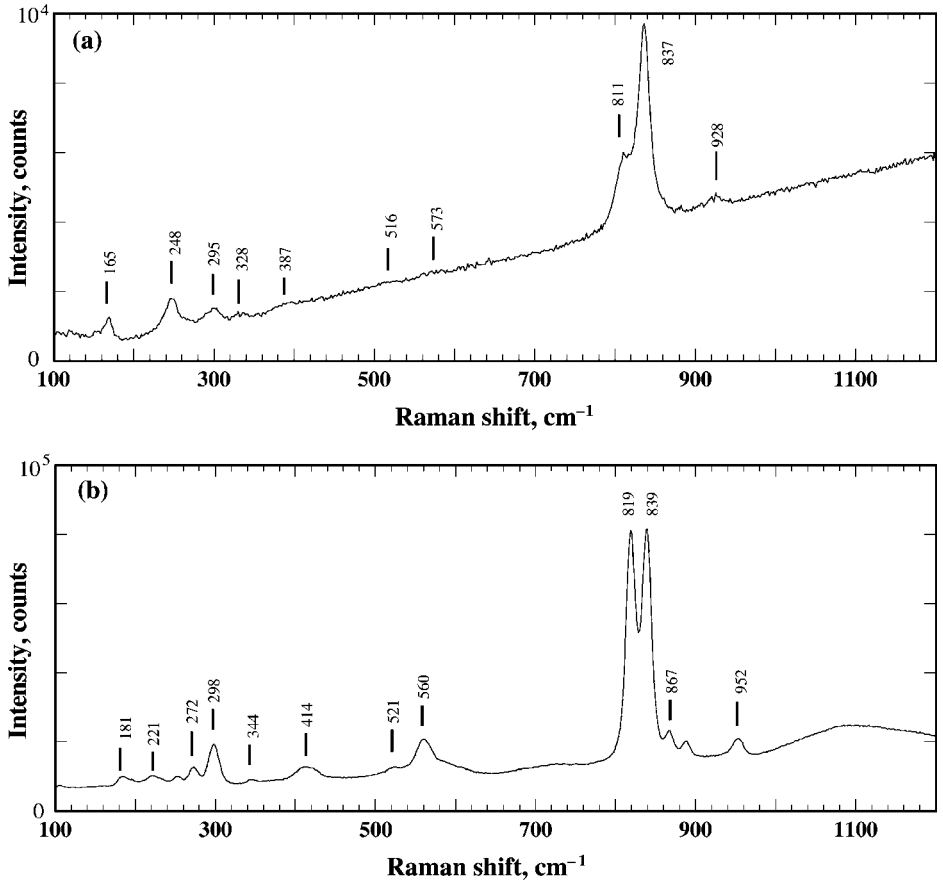


**FIG. 3.** The typical ambient Raman spectrum of (a) Co-olivine and (b) Ni-olivine. Note that the intensity scale in (a) is only 1/10th of that in (b).

the Raman modes corresponding to the ambient bands of Ni-olivine at 181, 221, 332, 344, and 414 $cm^{-1}$, respectively. From Table 1, bands 1 and 2 are lattice modes, 3 is a rotation mode, and 5 is an internal mode. Band 4 may be a rotation mode (19) or a lattice mode (21). In Fig. 5, all the vibrational frequencies of forsterite are higher than those of the corresponding modes of γ-$Ca_2SiO_4$. This case can be ascribed to larger unit cell in calcio-olivine. On the other hand, the frequencies of lattice modes 1, 2, and 4 appear to have a systematic variation with radius and CFSE of the cation in the olivine structure. Thus, a clear picture for the effect of increasing CFSE on the vibrational frequency cannot be obtained because decrease of cationic radius also results in the same trend. Nevertheless, the same trend was not observed in band 5 and other high-frequency internal modes of $SiO_4$. The reason for the absence of a relationship in vibrational frequency of the $SiO_4$-internal modes can be attributed to the weak effect of M2 cation substitution on the vibrations of $SiO_4$ (note that only one M2 octahedron is attached to $SiO_4$). Based on Raman spectra of forsterite, fayalite, and monticellite ($CaMgSiO_4$), Chopelas (21) attributed the lowering in Raman frequency of the $SiO_4$-internal modes to the increase in cation mass rather than the increase in unit cell volume. However, the present results do not support her argument.

## 4. CONCLUSIONS

Cobalt- and nickel-olivines and their solid solutions have been synthesized and studied by using X-ray diffraction and vibrational spectroscopy. $Co^{2+}$ appears to be helpful for the formation and crystal growth of the $(Co, Ni)_2SiO_4$ olivines. The results of X-ray diffraction indicate that Co- and Ni-olivines can form a continuous series of substitutional solid solutions, in which the *a*-axis shows the smallest expansion by substitution of $Co^{2+}$ for $Ni^{2+}$. The relationships between composition and lattice parameters are nearly linear. On the other hand, nearly all infrared and Raman frequencies show linear composition relationship, indicating that both $Co^{2+}$ and $Ni^{2+}$ distribute randomly over the M1 and M2 sites in the $(Co, Ni)_2SiO_4$ solid solutions. The linear composition dependences observed in the lattice parameters and vibrational frequencies have indicated that the mixing of cations in the $(Co, Ni)_2SiO_4$ solid solutions are nearly ideal.

The intensity of Raman spectra of the $(Co, Ni)_2SiO_4$ solid solutions decreases with increasing the amount of $Co_2SiO_4$.

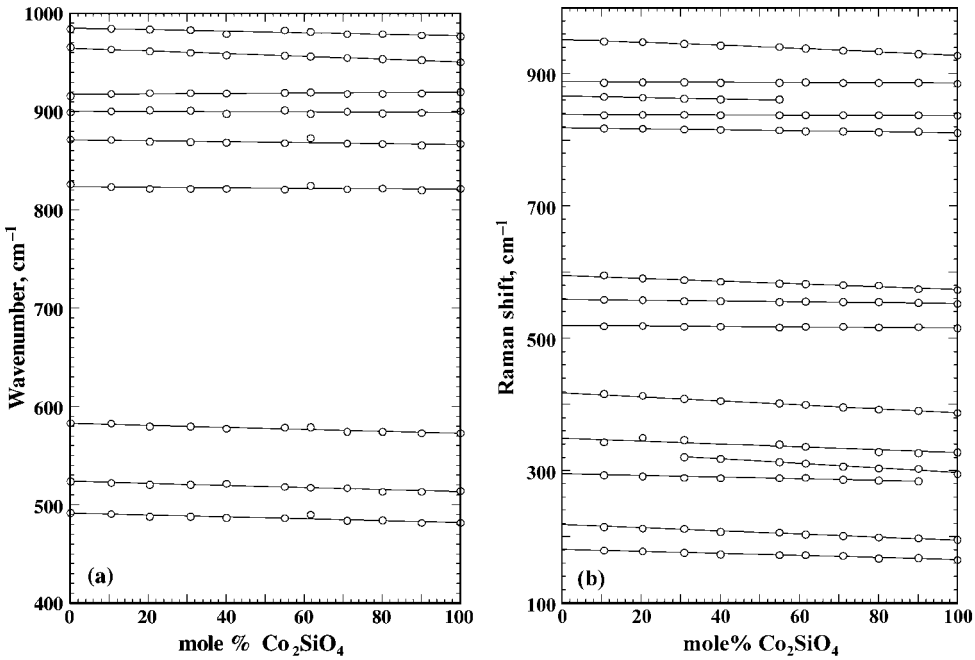


**FIG. 4.** The vibrational frequency-composition plots of $(Co, Ni)_2SiO_4$ solid solutions: (a) infrared modes and (b) Raman modes.

This case has been attributed to smaller electronegativity and larger average atomic weight for cobalt and thus smaller polarizability in vibrations of olivines after substitution of $Co^{2+}$ for $Ni^{2+}$. Together with other transition-metal silicate olivines, vibrational frequencies of the lattice Raman modes appear to have a systematic variation with radius and CFSE of cation in the olivine structure, while the same trend has not been observed in the $SiO_4$ internal modes. The reason for the absence of a relationship between the same internal modes of the transition-metal olivines may be chiefly attributed to the weak effect of cation substitution on the vibrations of $SiO_4$.

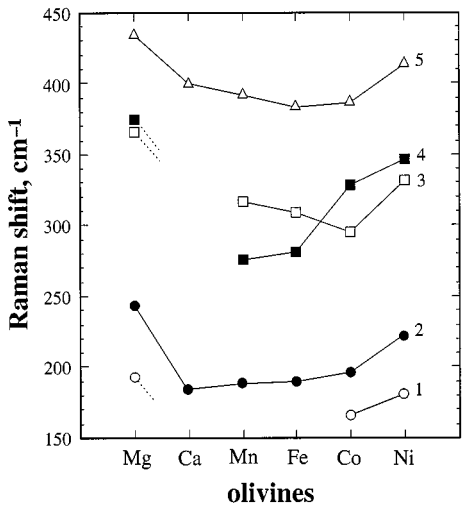


**FIG. 5.** The low-frequency Raman frequencies of six silicate olivines. 1, 2, 3, 4, and 5 represent the modes corresponding to the ambient bands of Ni-olivine at 181, 221, 332, 344, and 414 $cm^{-1}$, respectively. The uncertainties of frequencies are smaller than the size of symbols.

## ACKNOWLEDGMENTS

This work was supported by NSC Grant 88-2116-M-001-035. The author thanks Mr. H. D. Chiang, Institute of Materials Science and Engineering of National Sun Yat-Sen University, for analyzing the composition of the samples.

## REFERENCES

1. W. A. Deer, R. A. Howie, and J. Zussman, "An Introduction to the Rock-Forming Minerals," pp. 3–13. Longman Sci. and Tech., Essex, 1992.
2. V. Rajamani, G. E. Brown, and C. T. Prewitt, *Am. Mineral.* **60,** 292 (1975).
3. O. Tamada, *Mineral. J.* **10,** 71 (1980).
4. G. E. Brown, Jr., *in* "Orthosilicates" (P. H. Ribbe, Ed.), Chap. 11, pp. 275–381 and the literature cited therein. Mineralogical Society of America, Washington, DC, 1982.
5. M. Miyake, H. Nakamura, H. Kojima, and F. Marumo, *Am. Mineral.* **72,** 594 (1987).
6. R. G. Burns, "Mineralogical Application of Crystal Field Theory," Chap. 6, pp. 240–271. Cambridge Univ. Press, Cambridge, 1993.
7. B. A. Kolesov and J. V. Tanskaya, *Mater. Res. Bull.* **31,** 1035 (1996).
8. D. L. Bish, *Am. Mineral.* **66,** 770 (1981).
9. H. Annersten, T. Ericsson, and A. Filippidis, *Am. Mineral.* **67,** 1212 (1982).

10. R. D. Shannon, *Acta Crystallogr. A* **32,** 751 (1976).
11. F. E. Huggins, *Chem. Geol.* **11,** 99 (1973).
12. F. Guyot, H. Boyer, M. Madon, B. Velde, and J. P. Poirier, *Phys. Chem. Minerals* **13,** 91 (1986).
13. S. Akimoto and Y. Sato, *Phys. Earth Planet. Inter.* **1,** 498 (1968).
14. Y. Matsui and Y. Syono, *Geochem. J.* **2,** 51 (1968).
15. N. Morimoto, M. Tokonami, M. Watanabe, and K. Koto, *Am. Mineral.* **59,** 475 (1974).
16. W. D. Kingery, H. K. Bowen, and D. R. Uhlmann, "Introduction to Ceramics," Chap. 4, pp. 125–175. Wiley, New York, 1976.
17. L. Zhang, *Phys. Chem. Minerals* **25,** 308 (1998).
18. I. R. Bonilla, *J. Quant. Spectrosc. Radiat. Transfer* **38,** 527 (1982).
19. K. Iishi, *Am. Mineral.* **63,** 1198 (1978).
20. A. M. Hofmeister, *Phys. Chem. Minerals* **14,** 499 (1987).
21. A. Chopelas, *Am. Mineral.* **76,** 1101 (1991).
22. S. Y. Wang, S. K. Sharma, and T. F. Cooney, *Am. Mineral.* **78,** 469 (1993).
23. K. Mohanan, S. K. Sharma, and F. C. Bishop, *Am. Mineral.* **78,** 42 (1993).
24. R. G. Burns and F. E. Huggins, *Am. Mineral.* **57,** 967 (1972).
25. S. Ghose and C. Wan, *Contrib. Mineral. Petrol.* **47,** 131 (1974).
26. S. Ghose, C. Wan, F. Okamura, H. Ohashi, and J. R. Weidner, *Acta Crystallogr. A* **31,** S76 (1975).
27. G. E. Brown, Jr., and C. T. Prewitt, *Am. Mineral.* **58,** 577 (1973).
28. J. R. Smyth and R. M. Hazen, *Am. Mineral.* **58,** 588 (1973).
29. N. Aikawa, M. Kumazawa, and N. Tokonami, *Phys. Chem. Minerals* **12,** 1 (1985).
30. D. Ganguli, *N. Jb. Mineral. Abh.* **130,** 303 (1977).